

RESEARCH ARTICLE | MARCH 12 2025

Cryogenic magnetocaloric effect of rare-earth halide perovskites CsEuCl₃ and CsEuBr₃

Special Collection: [Multicalorics II](#)

Bingjie Wang; Fengxia Hu  ; Jing Wang ; Jirong Sun ; Tongyun Zhao; Baogen Shen

 Check for updates

J. Appl. Phys. 137, 103902 (2025)

<https://doi.org/10.1063/5.0235949>



Articles You May Be Interested In

Cs Eu Br 3 : Crystal structure and its role in the photostimulation of Cs Br : Eu 2 +

J. Appl. Phys. (October 2006)

Extreme learning machine and swarm-based support vector regression methods for predicting crystal lattice parameters of pseudo-cubic/cubic perovskites

J. Appl. Phys. (June 2020)

Cryogenic magnetocaloric effect of rare-earth halide perovskites CsEuCl₃ and CsEuBr₃

Cite as: J. Appl. Phys. 137, 103902 (2025); doi: 10.1063/5.0235949

Submitted: 30 August 2024 · Accepted: 18 February 2025 ·

Published Online: 12 March 2025



Bingjie Wang,^{1,2} Fengxia Hu,^{1,2,3,a)} Jing Wang,^{1,2} Jirong Sun,^{1,2,3} Tongyun Zhao,^{1,4} and Baogen Shen^{1,2,4,5}

AFFILIATIONS

¹Beijing National Laboratory for Condensed Matter Physics, Institute of Physics, Chinese Academy of Sciences, Beijing 100190, People's Republic of China

²School of Physical Sciences, University of Chinese Academy of Sciences, Beijing 101408, People's Republic of China

³Songshan Lake Materials Laboratory, Dongguan, Guangdong 523808, People's Republic of China

⁴Ganjiang Innovation Academy, Chinese Academy of Sciences, Ganzhou, Jiangxi 341000, People's Republic of China

⁵Ningbo Institute of Materials Technology & Engineering, Chinese Academy of Sciences, Ningbo, Zhejiang 315201, People's Republic of China

Note: This paper is part of the special topic, Multicalorics II.

a) Author to whom correspondence should be addressed: fxhu@iphy.ac.cn

ABSTRACT

Adiabatic demagnetization refrigeration (ADR) offers a compelling alternative to traditional ultra-low temperature technologies by eliminating the reliance on scarce ³He and gravitational constraints. The key of ADR development is to find magnetic refrigerants with exceptional magnetocaloric properties. In this study, polycrystalline CsEuCl₃ and CsEuBr₃ halide perovskites were synthesized by a simple solid-phase reaction method. CsEuCl₃ crystallizes in a tetragonal structure, while CsEuBr₃ forms an orthorhombic structure, both exhibiting distorted perovskite structures. CsEuCl₃ undergoes an antiferromagnetic ordering at $T_N \sim 1.1$ K, whereas CsEuBr₃ shows no magnetic ordering above 0.4 K. Curie–Weiss fitting analysis reveals antiferromagnetic interactions in both compounds, with CsEuBr₃ displaying stronger antiferromagnetic coupling. The maximum magnetic entropy change ($-\Delta S_M$) values under magnetic field changes of 0–2 T and 0–5 T are 22.4 and 38.6 J kg⁻¹ K⁻¹ at 1.4 K for CsEuCl₃, and 15.7 and 26.4 J kg⁻¹ K⁻¹ at 0.4 K for CsEuBr₃, respectively. These findings underscore the potential of CsEuCl₃ and CsEuBr₃ as promising candidates for cryogenic magnetic refrigeration applications.

© 2025 Author(s). All article content, except where otherwise noted, is licensed under a Creative Commons Attribution-NonCommercial-NoDerivs 4.0 International (CC BY-NC-ND) license (<https://creativecommons.org/licenses/by-nc-nd/4.0/>). <https://doi.org/10.1063/5.0235949>

I. INTRODUCTION

With the development of space exploration, quantum technology, and other frontier scientific research fields, the strong dependence on ³He for cryogenic technologies poses significant challenges due to its scarcity and high expense.^{1–3} Adiabatic demagnetization refrigeration (ADR), utilizing the magnetocaloric effect (MCE), offers an effective alternative for achieving cryogenic temperatures without the need for rare helium.^{4–7} The advantages of ADR, including enhanced reliability, compactness, simplicity, and the ability to control temperatures more accurately and consistently, alleviate concerns about helium shortages and make ADR particularly valuable in applications such as gas liquefaction, cooling in space missions, supporting advanced quantum computation, conducting cold atom

experiments, and achieving low-temperature superfluid phases.⁴ Thus, there is an urgent necessity to investigate various cryogenic refrigerants with significant MCE for use in ADR.

High-performance MCE materials typically exhibit characteristics such as magnetic ions with a large ground-state spin (J), weak magnetic anisotropy, weak magnetic interaction, and high magnetic density.^{8–12} Given that Gd³⁺ ions exhibit large $J = S = 7/2$, magnetic isotropy, and achievable low magnetic ordering temperatures, Gd-based compounds are attractive as magnetic refrigerants. Over recent decades, extensive research into Gd-based materials and device has been conducted.^{13–24} Notable examples include Gd₃Ga₅O₁₂ (GGG),¹⁹ Gd(HCOO)₃,²⁰ Gd(OH)F₂,²¹ GdPO₄,²² and the molecular {Gd₁₂Na₆} quadruple-wheel.²³

12 June 2025 13:08:32

Similarly, Eu^{2+} ions, which share the same J -value and magnetic isotropy as Gd^{3+} ions, have garnered interest. Despite the limited research focused on the MCE of Eu^{2+} -based materials, especially at cryogenic temperatures, certain materials have shown promising magnetocaloric performances. Notably, $\text{Eu}_2\text{B}_2\text{O}_5$,⁵ and EuB_2O_4 ²⁶ have reported significant magnetic entropy change ($-\Delta S_M$) values of $13.7 \text{ J kg}^{-1} \text{ K}^{-1}$ at 2.7 K and $19.4 \text{ J kg}^{-1} \text{ K}^{-1}$ at 1.3 K under magnetic field change of $H = 0\text{--}1 \text{ T}$, respectively. However, the quest for more Eu^{2+} -based materials that exhibit substantial MCE at cryogenic temperatures and under lower magnetic fields continues to be challenging.

Halide perovskites have garnered significant interest due to their unique electrical and optical properties at low temperatures.^{27–31} These halide perovskites, incorporating rare-earth ions, allow for the creation of three-dimensional magnetic halide perovskites such as CsEuX_3 ($X = \text{Cl}, \text{Br}, \text{and I}$) have been synthesized.^{32–35} However, reports on their magnetocaloric performances are limited. Notably, only the lattice constants of polycrystalline CsEuI_3 have been reported so far, lacking a well-defined space group,³⁵ and its relatively low magnetic density (22.0%) suggests a small theoretical limit $-\Delta S_M = nR \ln(2S + 1)/M_W$. Consequently, this study focuses on CsEuCl_3 and CsEuBr_3 , which have higher magnetic densities of 38.9% and 29.0%, respectively, correlating with larger theoretical limit $-\Delta S_M$ may result in larger achieved $-\Delta S_M$ than CsEuI_3 .

Here, magnetocaloric studies were conducted on CsEuCl_3 and CsEuBr_3 . CsEuCl_3 crystallizes in a tetragonal structure, forming a distorted perovskite, while CsEuBr_3 with an orthorhombic structure, exhibits more distortion. CsEuCl_3 undergoes a magnetic ordering transition from the antiferromagnetic (AFM) to paramagnetic (PM) at $T_N \sim 1.1 \text{ K}$, while no magnetic ordering is observed in CsEuBr_3 down to 0.4 K. Dominant AFM interactions in both compounds are confirmed by Curie–Weiss fits and Brillouin function analysis. The maximum $-\Delta S_M$ values under $H = 0\text{--}2 \text{ T}$ are $22.4 \text{ J kg}^{-1} \text{ K}^{-1}$ at 1.4 K for CsEuCl_3 and $15.7 \text{ J kg}^{-1} \text{ K}^{-1}$ at 0.4 K for CsEuBr_3 . Under $H = 0\text{--}5 \text{ T}$, the maximum $-\Delta S_M$ values are 38.6 and $26.4 \text{ J kg}^{-1} \text{ K}^{-1}$, respectively. These results demonstrate that halide perovskites CsEuCl_3 and CsEuBr_3 exhibit substantial cryogenic MCE, positioning them as promising candidates for cryogenic magnetic refrigeration.

II. EXPERIMENTAL DETAILS

Polycrystalline samples of CsEuCl_3 and CsEuBr_3 were synthesized via a simple solid-phase reaction. EuCl_2 powder with 99.99% purity was obtained from Aladdin. EuBr_2 with 99.99% purity and CsX ($X = \text{Cl}, \text{Br}$) with 99.998% purity were obtained from ALFA. All procedures were carried out in an argon-filled glovebox, maintaining H_2O and O_2 levels $<0.1 \text{ ppm}$ to prevent contamination. Stoichiometric quantities of EuCl_2 and CsCl , as well as EuBr_2 and CsBr , were accurately weighed and mixed in a 1:1 molar ratio. These homogeneous mixtures were then transferred into quartz tubes. The tubes were subsequently evacuated to a high vacuum to eliminate air and any other gases that could affect the reaction, and then sealed. The sealed tubes were placed in a muffle furnace and heated at a rate of $5^\circ\text{C}/\text{min}$ to 500°C , where they were maintained

for 8 h to ensure complete reaction, followed by natural cooling to room temperature.

CsEuCl_3 and CsEuBr_3 samples were always stored in an argon-filled glovebox with oxygen and water levels below 1 ppm to minimize oxidation. The crystal structures of the samples were characterized using x-ray diffraction (XRD, Rigaku Smartlab) with a $\text{Cu-K}\alpha$ target ($\lambda = 1.5406 \text{ \AA}$). To prevent any oxidation of the Eu^{2+} ions, the samples were carefully sealed with Kapton films inside the glovebox before XRD measurements. This precaution ensured that the samples were not exposed to air throughout the XRD measurements. Rietveld refinement analysis was performed using the general structure analysis system (GSAS) suite to determine detailed crystallographic information. Magnetic measurements were performed using a Quantum Design MPMS-3 superconducting quantum interference device (SQUID) magnetometer, with a temperature range from 1.8 to 300 K. The ultralow-temperature magnetization data from 0.4 to 2 K were measured using a DC MPMS-3 equipped with a ^3He -refrigerator insert. Samples for magnetic measurements were mounted to the holders in the glovebox.

III. RESULTS AND DISCUSSION

The room temperature XRD patterns and the Rietveld refinements for CsEuCl_3 and CsEuBr_3 are shown in Figs. 1(a) and 1(b). The XRD analysis for CsEuCl_3 [Fig. 1(a)] confirms the sample is in a single phase, with no detectable secondary phase present. However, there is a small amount of residual CsBr ($\sim 3\%$) in the CsEuBr_3 sample [Fig. 1(b)]. The Rietveld refinement suggests that CsEuCl_3 crystallizes in a tetragonal structure with space group $P4/\text{mbm}$, having lattice parameters $a = b = 7.8969 \text{ \AA}$, and $c = 5.6211 \text{ \AA}$. Conversely, CsEuBr_3 adopts an orthorhombic structure with space group Pbnm and lattice parameters $a = 8.2172 \text{ \AA}$, $b = 8.2902 \text{ \AA}$, and $c = 11.7854 \text{ \AA}$, respectively. These results align with previously reported data,³² and the detailed refinement results are summarized in Table I.

For ABX_3 -type perovskites, structural stability is often assessed using the tolerance factor t , calculated by the formula $t = \frac{r_A + r_X}{\sqrt{2}(r_B + r_X)}$. An ideal perovskite structure typically indicated by a t value close to 1, suggests well-matched ionic sizes that favor for ideal cubic symmetry. Deviations of t value from 1, either $t < 1$ or $t > 1$, are caused by the relatively small or large size of the B-site ion, leading to structural distortion such as tetragonal or orthorhombic formations. The calculated tolerance factors for CsEuCl_3 and CsEuBr_3 are approximately 0.841 and 0.835, respectively, both less than 1. These values indicate that the B-site ions (Eu^{2+}) are relatively small, promoting deviations from the ideal cubic symmetry and resulting in tetragonal or orthorhombic structures, which are confirmed by XRD analysis for CsEuCl_3 and CsEuBr_3 . The schematics of crystal structure for CsEuCl_3 and CsEuBr_3 are illustrated in Figs. 1(c) and 1(d). Notably, in the perovskite structure, magnetic Eu^{2+} ions occupy the B-site, with each Eu^{2+} ion surrounded by six Cl^- or Br^- ions in an octahedral arrangement, illustrated by the pink polyhedron in Figs. 1(c) and 1(d). The Cs^+ ions are situated in the A-sites, filling the large cavities formed by the connected octahedra, which assist in stabilizing the lattice through ionic interactions and size effects. The larger ionic radius of Br^- results in a more distorted perovskite structure for CsEuBr_3 compared to CsEuCl_3 .

12 June 2025, 13:08:32

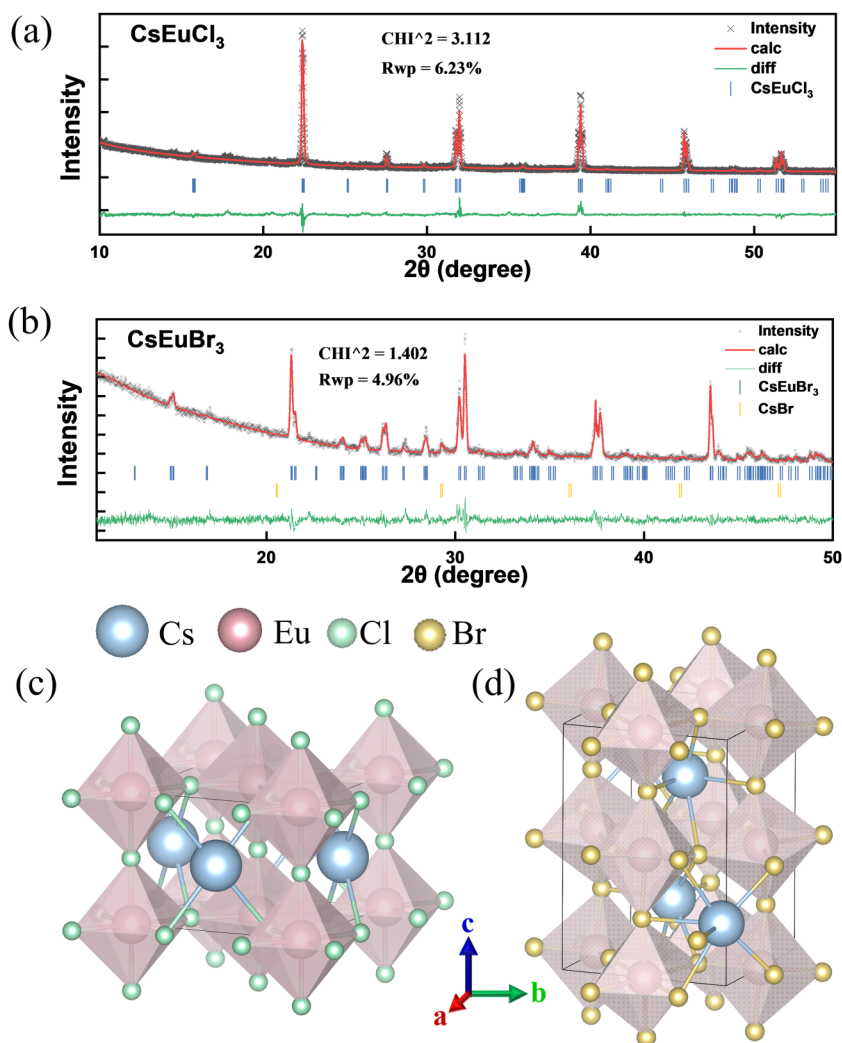


FIG. 1. Powder XRD patterns with Rietveld refinements and differences for (a) CsEuCl_3 , and (b) CsEuBr_3 . Perspective view of crystallographic structure for (c) CsEuCl_3 and (d) CsEuBr_3 .

Moreover, CsEuCl_3 has $159.0(4)^\circ$ and 180° inter-octahedral Eu–Cl–Eu bond angles, while CsEuBr_3 has $154.25(31)^\circ$ and $161.2(4)^\circ$ inter-octahedral Eu–Br–Eu bond angles. The structural distortions observed in both CsEuCl_3 and CsEuBr_3 further influence their physical properties, particularly affecting their magnetic characteristics.

Magnetic measurements were conducted to ascertain the magnetic properties and magnetocaloric effects of CsEuCl_3 and CsEuBr_3 . Measurements above 1.8 K were collected on the MPMS-3 system, while ultra-low temperature measurements from 1.8 to 0.4 K were conducted by ^3He -insert in the MPMS-3 system. Figures 2(a) and 2(b) plot the temperature-dependent magnetization (M - T) of these compounds under both zero-field cooling (ZFC) and field cooling (FC) conditions, with an applied magnetic field of 0.01 T from 0.4 to 300 K. In the high-temperature range, both CsEuCl_3 and CsEuBr_3 exhibit nearly constant magnetization with no obvious difference between the ZFC and FC curves. As shown in Fig. 2(a), when the temperature of CsEuCl_3 decreases, its

M - T curve peaks at approximately 1.1 K, indicating a magnetic phase transition from PM to AFM state at $T_N \sim 1.1$ K. In contrast, for CsEuBr_3 [Fig. 2(b)], there is a broad feature with a maximum around ~ 1.3 K, accompanied by a slight bifurcation between the ZFC and FC below this temperature. This behavior may suggest the possibility of magnetic ordering. However, as the temperature decreases further below 1.3 K, magnetization continues to increase, indicating that a significant portion of the sample remains in a PM state. This PM component likely contributes to the dominant signal at lower temperatures. Therefore, the anomaly observed around 1.3 K may be indicative of short-range magnetic ordering in CsEuBr_3 , although further investigation is still required to confirm this hypothesis. In previous literature,³² antiferromagnetic ordering temperature around 2.0 K for CsEuBr_3 was detected from heat capacity measurements. This discrepancy may be due to the possible differences in sample preparation and/or measurement techniques. Figures 2(c) and 2(d) depict the temperature-dependent reciprocal susceptibility ($1/\chi = H/M$) for CsEuCl_3 and CsEuBr_3 .

TABLE I. Lattice parameters and Rietveld refinement factors for CsEuCl₃ and CsEuBr₃.

Compounds	CsEuCl ₃	CsEuBr ₃
F.W. (g/mol)	391.22	524.6
Space group	P 4/mbm	P bnm
Temperature (K)	300	300
a (Å)	7.8969(1)	8.2172(6)
b (Å)	7.8969(1)	8.2902(5)
c (Å)	5.6211(1)	11.7854(8)
V (Å ³)	350.541(20)	802.849(148)
R _{wp}	0.0623	0.0496
χ ²	3.112	1.402

In the paramagnetic (PM) region, the behavior of these compounds obeys the Curie–Weiss law, expressed as $\chi = \frac{N(\mu_B \mu_{\text{eff}})^2}{3K_B(T - \theta_{\text{CW}})} + \chi_0$, where K_B is the Boltzmann constant, θ_{CW} is the paramagnetic Curie temperature, μ_{eff} is the effective magnetic moment, μ_B is the Bohr magneton, and χ_0 denotes the temperature-independent contribution

and accounts for a magnitude of $10^{-3} \text{ emu mol}^{-1} \text{ Oe}^{-1}$. The determined effective magnetic moment μ_{eff} for CsEuCl₃ and CsEuBr₃ are $7.85 \mu_B$ and $8.58 \mu_B$, respectively. Comparatively, the theoretical effective moment for a free Eu²⁺ ion ($J = S = 7/2, L = 0$), calculated as $7.94 \mu_B$ based on $g_J \sqrt{J(J+1)}$, where the Landé g-factor g_J is 2. The experimental value (μ_{eff}) of CsEuCl₃ aligns closely with the theoretical spin-only moment of Eu²⁺ ($7.94 \mu_B$), whereas μ_{eff} of CsEuBr₃ is slightly higher than $7.94 \mu_B$, potentially due to stronger interactions and crystal effects. Furthermore, θ_{CW} for CsEuCl₃ and CsEuBr₃ are -3.00 and -4.30 K, respectively. These negative θ_{CW} suggest that AFM interactions predominate in these compounds. Typically, $|\theta_{\text{CW}}|$ values reflect the strength of magnetic interactions, with smaller values indicating weaker magnetic interaction.^{8,36,37} CsEuBr₃, with its larger $|\theta_{\text{CW}}|$, exhibits stronger AFM couplings, possibly resulting from its more distorted perovskite structures. This relatively pronounced AFM coupling in CsEuBr₃ could potentially lead to a weaker MCE.³⁶

To further investigate the magnetic properties of CsEuCl₃ and CsEuBr₃, magnetizations at 0.4 K obtained from experiments were compared with predictions from the free Heisenberg spin model. This model provides a robust framework for describing

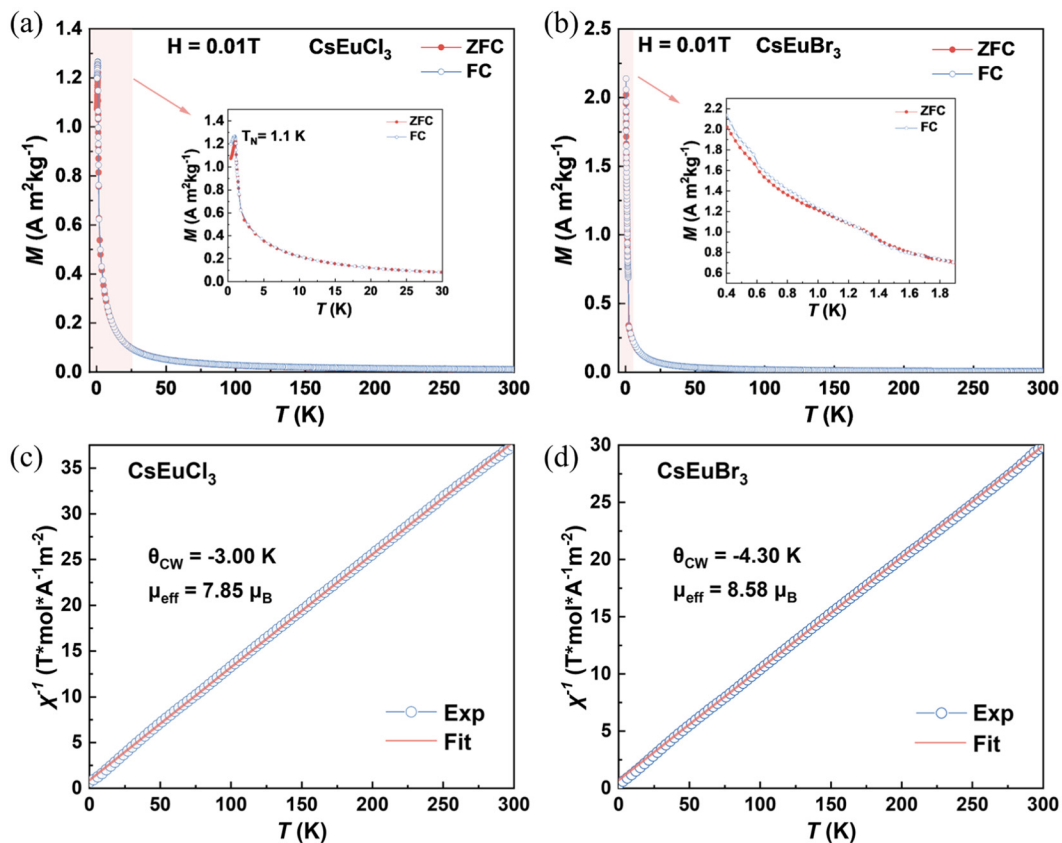


FIG. 2. Temperature dependence (M – T curve) of zero-field cooling (ZFC) and field cooling (FC) curves from 0.4 to 300 K at $H = 0.01$ T for (a) CsEuCl₃ and (b) CsEuBr₃. The insets give the enlarged M – T curves under low temperatures. The temperature-dependent reciprocal susceptibility ($1/\chi = H/M$) for (c) CsEuCl₃ and (d) CsEuBr₃.

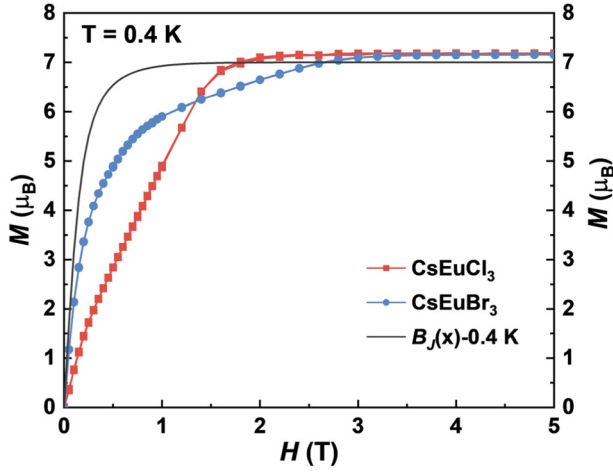


FIG. 3. Field-dependent magnetization in 0.4 K for CsEuCl₃ and CsEuBr₃, and the Brillouin-like free spins $B_J(x)$ of free Eu²⁺ ions at $T=0.4$ K.

magnetization M under an applied magnetic field H and at a specific temperature T . Magnetization is expressed by the form^{38,39}

$$M = M_0 B_J(x), \quad (1)$$

where M_0 is the saturation magnetization, defined as $M_0 = Jg_l\mu_B$, and $B_J(x)$ is the Brillouin function. Here, x is a variable given by $x = Jg_l\mu_B\mu_0 H/k_B T$, with $J = S = 7/2$ and $g_l = 2$ for Eu²⁺ ions. The Brillouin function $B_J(x)$ is described by

$$B_J(x) = \frac{1}{2J} \left[(2J + 1) \coth \frac{2J + 1}{2J} x - \coth \frac{x}{2J} \right]. \quad (2)$$

This function models the magnetization behavior of an ideal paramagnet where spin interactions are minimal. The Brillouin function for a single magnetically uncoupled Eu²⁺ ion with $S = 7/2$ and $g_l = 2$ at $T = 0.4$ K was calculated.

Figure 3 illustrates the M - H curves for CsEuCl₃ and CsEuBr₃ from magnetic measurements alongside the $B_J(x)$ curve at 0.4 K. The observed magnetization increases slowly at low fields and does not reach saturation even at 5 T, indicative of typical AFM properties at low temperatures. A clear divergence between the M - H curves of both CsEuCl₃ and CsEuBr₃, and the Brillouin function is evident, highlighting significant spin-spin interactions within these compounds.

Further investigations into magnetocaloric performance of CsEuCl₃ and CsEuBr₃ were conducted through isothermal M - H curves measured from 1.8 to 20 K, as given in Figs. 4(a) and 4(d), and the ultralow temperature measurements from 1.8 to 0.4 K, as given in Figs. 4(b) and 4(e). The isothermal M - H curves for both CsEuCl₃ and CsEuBr₃ exhibit AFM characteristics. Notably, the

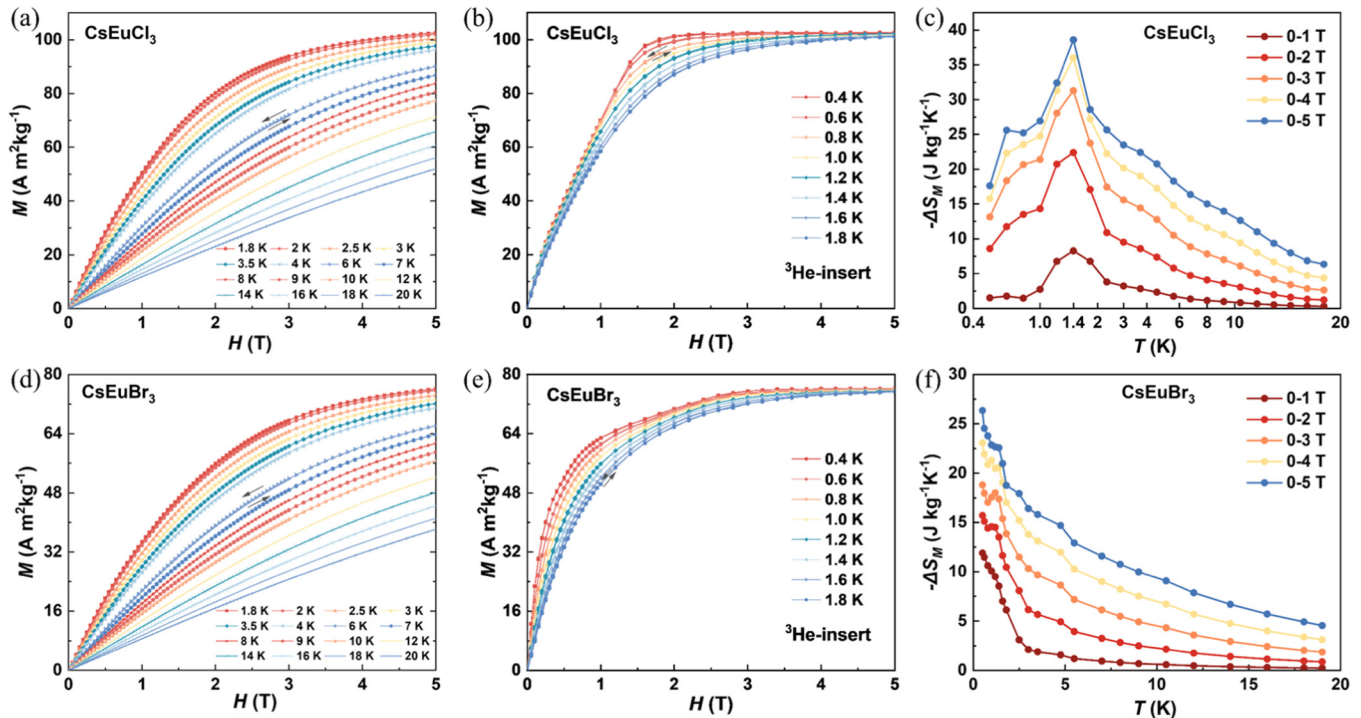


FIG. 4. Magnetocaloric effect. Isothermal magnetization curves (M - H) from 0 to 5 T for (a) and (b) CsEuCl₃ and (d) and (e) CsEuBr₃ from 1.8 to 20 K and 0.4 to 1.8 K. The temperature-dependent $-\Delta S_M$ curves from 0.4 to 20 K under magnetic field change of 0–1 T to 0–5 T for (c) CsEuCl₃ and (f) CsEuBr₃.

12 June 2025 13:08:32

TABLE II. Comparison of magnetocaloric parameters of CsEuCl₃ and CsEuBr₃ with some Gd-/Eu-based magnetocaloric materials.^{16,19,25,26,41–47} The parameters include magnetic order temperature T_{ord} , the experimental $|\Delta S_M^{\text{exp}}|$ at $H=0-2$ T and $H=0-5$ T, magnetic density M_R/M_W (M_R and M_W represent the weight of magnetic elements and compound, respectively), the theoretical $|\Delta S_M^{\text{the}}|$ from $-\Delta S_M = nR \ln(2J+1)/M_W$, and the ratio of the experimental $|\Delta S_M^{\text{exp}}|$ at $H=0-5$ T to the theoretical $|\Delta S_M^{\text{the}}|$ denoted as $-\Delta S_M^{\text{ST}}/-\Delta S_M^{\text{the}}$.

Compound	T_{ord} (K)	θ_{CW} (K)	$ \Delta S_M^{\text{exp}} $ (J kg ⁻¹ K ⁻¹)		$\frac{M_R}{M_W}$	Theoretical $ \Delta S_M^{\text{the}} $ (J kg ⁻¹ K ⁻¹)	$\frac{-\Delta S_M^{\text{ST}}}{-\Delta S_M^{\text{the}}}$	Reference
			0–2 T	0–5 T				
CsEuCl ₃	1.1	−3.0	22.4	38.6	38.9%	44.2	87.3%	This work
CsEuBr ₃	<0.4	−4.3	15.7	26.4	29.0%	33.0	80.0%	This work
Gd ₂ FeAlO ₆	<2	...	5.2	~19	63.6%	70.1	27.1%	41
Sr ₂ GdNbO ₆	2.0	3.18	16.4	26.1	30.1%	33.1	78.9%	42
Gd ₂ MgTiO ₆	~3.3	−5.6	6.1	33.8	65.1%	71.6	48.9%	43
Gd ₂ NiTiO ₆	4.0	...	6.9	31.3	60.7%	66.8	46.8%	44
EuTiO ₃	5.6	3.2	22.3	44.4	61.3%	69.7	63.7%	45
Gd ₂ Ti ₂ O ₇	<2	−13.4	3.4	17.9	60.3%	66.2	27.0%	46
GdBO ₃	1.7	−5.4	7.5	36	72.8%	80.0	45.0%	47
Gd(OH) ₃	0.94	−1.7	26.9	56	75.5%	83.0	67.5%	16
Gd ₃ Ga ₅ O ₁₂	0.8	...	~21	~35	46.6%	51.2	68.4%	19
EuB ₂ O ₄	0.72	−3.6	35.0	50.8	63.9%	72.7	69.9%	26
Eu ₂ B ₂ O ₅	2.7	0.47	28.2	46.9	74.9%	85.2	55.0%	25

M - H curves for increasing and decreasing magnetic fields are reversible, as shown by the arrows in Fig. 4, which indicates that both CsEuCl₃ and CsEuBr₃ have excellent magnetic reversibility. According to the Maxwell equation $\Delta S_M(T, H) = \int_0^{H_{\text{max}}} \left(\frac{\partial M}{\partial T}\right)_H dH$, the MCE for these compounds were calculated, and the temperature-dependent $-\Delta S_M$ under various magnetic fields are presented in Fig. 4(c) for CsEuCl₃ and Fig. 4(f) for CsEuBr₃. The maximum $-\Delta S_M$ values for CsEuCl₃ under $H=0-2$ T and $H=0-5$ T are 22.4 and 38.6 J kg⁻¹ K⁻¹ at 1.4 K, respectively, which are comparable to some reported cryogenic materials.^{19,40–44} For CsEuBr₃, the $-\Delta S_M$ - T curve has no peak within the temperature range from 0.4 to 20 K, and the maximum $-\Delta S_M$ values under $H=0-2$ T and $H=0-5$ T are 15.7, and 26.4 J kg⁻¹ K⁻¹ at 0.4 K, respectively.

Table II compares the magnetic parameters of CsEuCl₃ and CsEuBr₃ with other Gd³⁺- and Eu²⁺-based cryogenic magnetocaloric materials,^{16,19,25,26,41–47} providing experimental maximum $-\Delta S_M$ values at $H=0-2$ T and $H=0-5$ T along with the theoretical $-\Delta S_M$ values. For the Eu²⁺-based compounds, the theoretical limit calculated by $-\Delta S_M = nR \ln(2S+1)/M_W$ depends entirely on the magnetic density M_R/M_W , noting that Eu²⁺ ions have the same $J=S=7/2$, $L=0$ and magnetic isotropy with Gd³⁺ ions. However, experimentally achieved $-\Delta S_M$ and deviations from the corresponding theoretical $-\Delta S_M$ can vary due to specific coordination environments, which plays a pivotal role in affecting magnetic interaction, and hence the spin alignments under external fields. For CsEuCl₃ and CsEuBr₃, the magnetic density M_R/M_W are 38.9%, and 29.0%, respectively, and the corresponding theoretical $-\Delta S_M$ are 44.2 J kg⁻¹ K⁻¹ and 33.0 J kg⁻¹ K⁻¹, respectively. CsEuCl₃ at $H=0-5$ T achieves 87.3% of theoretical $-\Delta S_M$, whereas CsEuBr₃ reaches 80.0% of its theoretical $-\Delta S_M$. This difference may be attributed to variations in their coordination environment, for CsEuCl₃ with a less distorted perovskite structure and the relatively

weak AFM interactions, making the achieved $-\Delta S_M$ closer to theoretical $-\Delta S_M$.

In comparison, Gd₂Ti₂O₇,⁴⁶ with a higher magnetic density M_R/M_W of 60.3% compared to CsEuCl₃ and CsEuBr₃, achieves only 27.0% of its theoretical $-\Delta S_M$ at $H=0-5$ T. The lower $-\Delta S_M$ for Gd₂Ti₂O₇ is likely due to a more geometrically frustrated structure and stronger AFM couplings. This analysis underscores the significant impact of coordination environment and magnetic density on magnetocaloric performance. Though CsEuCl₃ and CsEuBr₃ do not outperform certain Eu- or Gd-based compounds, particularly those with higher magnetic densities and/or weaker magnetic interactions, $-\Delta S_M$ of CsEuCl₃ and CsEuBr₃ is still greater than or comparable with several perovskite-structured materials^{41–44} (Gd₂FeAlO₆, Sr₂GdNbO₆, Gd₂MgTiO₆, etc.). Notably, $-\Delta S_M$ for CsEuCl₃ under $H=0-2$ T is comparable to that of commercial cryogenic refrigerant Gd₃Ga₅O₁₂ (GGG)¹⁹ with $-\Delta S_M \sim 21$ J kg⁻¹ K⁻¹. Furthermore, for CsEuX₃ magnetic halide perovskites, replacing the Cs⁺ ions at the A-site with smaller and lighter organic cations could potentially increase the magnetic density. Simultaneously, such changes in the coordination environment could lead to lower magnetic ordering temperatures and weaker magnetic interactions, creating favorable conditions for achieving exceptional cryogenic MCE. Such alterations are promising and warrant further investigation.

IV. CONCLUSION

In conclusion, polycrystalline CsEuCl₃ and CsEuBr₃ were successfully synthesized using a solid-phase reaction method, and their crystal structures, magnetic properties, and magnetocaloric effects were investigated. CsEuCl₃ crystallizes in a tetragonal structure, whereas CsEuBr₃ crystallizes in an orthorhombic structure, forming a more distorted perovskite structure due to a larger ionic

radius of Br^- . CsEuCl_3 undergoes a magnetic ordering transition from AFM to PM state at around 1.1 K, whereas CsEuBr_3 exhibits no magnetic ordering above 0.4 K. Curie–Weiss analysis indicates stronger AFM interactions in CsEuBr_3 than in CsEuCl_3 , likely due to distinct coordination environments, which consequently influence their magnetocaloric effect. The maximum $-\Delta S_M$ values recorded for CsEuCl_3 and CsEuBr_3 at $H = 0\text{--}2$ T are $22.4 \text{ J kg}^{-1} \text{ K}^{-1}$ (1.4 K) and $15.7 \text{ J kg}^{-1} \text{ K}^{-1}$ (0.4 K), respectively, and at $H = 0\text{--}5$ T are 38.6 and $29.0 \text{ J kg}^{-1} \text{ K}^{-1}$, respectively. The promising magnetocaloric performances of CsEuCl_3 and CsEuBr_3 highlight their potential for applications in cryogenic magnetic refrigeration. This study lays the groundwork for future exploration of high-performance cryogenic magnetocaloric materials.

ACKNOWLEDGMENTS

This work was supported by the Science Center of the National Science Foundation of China (No. 52088101), the National Key Research and Development Program of China (Nos. 2021YFB3501202, 2020YFA0711500, and 2023YFA1406003), the National Natural Sciences Foundation of China (Nos. U23A20550, 92263202, and 22361132534), the Strategic Priority Research Program B (No. XDB33030200) of the Chinese Academy of Sciences (CAS), and the Synergetic Extreme Condition User Facility (SECUF).

AUTHOR DECLARATIONS

Conflict of Interest

The authors have no conflicts to disclose.

Author Contributions

Bingjie Wang: Data curation (lead); Formal analysis (lead); Investigation (lead); Methodology (lead); Writing – original draft (lead). **Fengxia Hu:** Conceptualization (equal); Funding acquisition (equal); Resources (equal); Supervision (equal); Writing – review & editing (equal). **Jing Wang:** Methodology (equal); Resources (equal); Supervision (equal). **Jirong Sun:** Methodology (equal); Resources (equal); Supervision (equal). **Tongyun Zhao:** Methodology (equal); Resources (equal); Supervision (equal). **Baogen Shen:** Funding acquisition (equal); Resources (equal); Supervision (equal).

DATA AVAILABILITY

The data that support the findings of this study are available from the corresponding author upon reasonable request.

REFERENCES

- ¹P. V. E. McClintock, “Will detente kill millikelvin research?,” *Nature* **276**(5684), 117 (1978).
- ²R. Stone, “Researchers rise to challenge of replacing helium-3,” *Science* **353**(6294), 15–16 (2016).
- ³A. Cho, “Helium-3 shortage could put freeze on low-temperature research,” *Science* **326**(5954), 778–779 (2009).
- ⁴P. J. Shirron, “Applications of the magnetocaloric effect in single-stage, multi-stage and continuous adiabatic demagnetization refrigerators,” *Cryogenics* **62**, 130–139 (2014).

- ⁵J.-M. Duval, P. Camus, M. Calvo, T. Prouvé, O. Exshaw, and D. P. Brasiliano, “Development of an ADR refrigerator with two continuous stages,” *J. Low Temp. Phys.* **184**(3–4), 604–608 (2016).
- ⁶K. Li, Y.-N. Wang, P. Liu, F.-Q. Yu, W. Dai, and J. Shen, “Experimental research on a 50 mK multi-stage adiabatic demagnetization refrigerator,” *Acta Phys. Sin.* **72**(19), 190702 (2023).
- ⁷P. Shirron, “Optimization strategies for single-stage, multi-stage and continuous ADRs,” *Cryogenics* **62**, 140–149 (2014).
- ⁸Y.-Z. Zheng, G.-J. Zhou, Z. Zheng, and R. E. P. Winpenny, “Molecule-based magnetic coolers,” *Chem. Soc. Rev.* **43**(5), 1462–1475 (2014).
- ⁹J.-L. Liu, Y.-C. Chen, F.-S. Guo, and M.-L. Tong, “Recent advances in the design of magnetic molecules for use as cryogenic magnetic coolants,” *Coord. Chem. Rev.* **281**, 26–49 (2014).
- ¹⁰X.-Y. Zheng, J. Xie, X.-J. Kong, L.-S. Long, and L.-S. Zheng, “Recent advances in the assembly of high-nuclearity lanthanide clusters,” *Coord. Chem. Rev.* **378**, 222–236 (2019).
- ¹¹B. Wang, X. Liu, F. Hu, J.-T. Wang, J. Xiang, P. Sun, J. Wang, J. Sun, T. Zhao, Z. Mo, J. Shen, Y. Chen, Q. Huang, and B. Shen, “A record-high cryogenic magnetocaloric effect discovered in EuCl_2 compound,” *J. Am. Chem. Soc.* **146**(51), 35016–35022 (2024).
- ¹²L. Xie, C. Liang, Y. Qin, H. Zhou, Z. Yu, H. Chen, M. Naeem, K. Qiao, Y. Wen, B. Zhang, G. Wang, X. Li, J. Liu, V. Franco, K. Chu, M. Yi, and H. Zhang, “High-throughput screening of high-performance magnetocaloric materials by gradient additive manufacturing,” *Adv. Funct. Mater.* **35**, 2414441 (2024).
- ¹³N. Xu, W. Chen, Y.-S. Ding, and Z. Zheng, “A cubic Tinkertoy-like heterometallic cluster with a record magnetocaloric effect,” *J. Am. Chem. Soc.* **146**(14), 9506–9511 (2024).
- ¹⁴X.-Y. Zheng, Y.-H. Jiang, G.-L. Zhuang, D.-P. Liu, H.-G. Liao, X.-J. Kong, L.-S. Long, and L.-S. Zheng, “A gigantic molecular wheel of $\{\text{Gd}_{140}\}$: A new member of the molecular wheel family,” *J. Am. Chem. Soc.* **139**(50), 18178–18181 (2017).
- ¹⁵X.-M. Luo, Z.-B. Hu, Q. Lin, W. Cheng, J.-P. Cao, C.-H. Cui, H. Mei, Y. Song, and Y. Xu, “Exploring the performance improvement of magnetocaloric effect based Gd-exclusive cluster Gd_{60} ,” *J. Am. Chem. Soc.* **140**(36), 11219–11222 (2018).
- ¹⁶Y. Yang, Q.-C. Zhang, Y.-Y. Pan, L.-S. Long, and L.-S. Zheng, “Magnetocaloric effect and thermal conductivity of $\text{Gd}(\text{OH})_3$ and $\text{Gd}_2\text{O}(\text{OH})_4(\text{H}_2\text{O})_2$,” *Chem. Commun.* **51**(34), 7317–7320 (2015).
- ¹⁷Q.-F. Xu, B.-L. Liu, M.-Y. Ye, L.-S. Long, and L.-S. Zheng, “Magnetocaloric effect and thermal conductivity of a 3D coordination polymer of $[\text{Gd}(\text{HCOO})(\text{C}_2\text{O}_4)]_n$,” *Inorg. Chem.* **60**(13), 9259–9262 (2021).
- ¹⁸N. Xu, W. Chen, Y.-S. Ding, and Z. Zheng, “A cubic tinkertoy-like heterometallic cluster with a record magnetocaloric effect,” *J. Am. Chem. Soc.* **146**(14), 9506–9511 (2024).
- ¹⁹B. Daudin, R. Lagnier, and B. Salce, “Thermodynamic properties of the gadolinium gallium garnet, $\text{Gd}_3\text{Ga}_5\text{O}_{12}$, between 0.05 and 25 K,” *J. Magn. Magn. Mater.* **27**(3), 315–322 (1982).
- ²⁰G. Lorusso, J. W. Sharples, E. Palacios, O. Roubeau, E. K. Brechin, R. Sessoli, A. Rossin, F. Tuna, E. J. L. McInnes, D. Collison, and M. Evangelisti, “A dense metal-organic framework for enhanced magnetic refrigeration,” *Adv. Mater.* **25**(33), 4653–4656 (2013).
- ²¹Q. Xu, B. Liu, M. Ye, G. Zhuang, L. Long, and L. Zheng, “ $\text{Gd}(\text{OH})\text{F}_2$: A promising cryogenic magnetic refrigerator,” *J. Am. Chem. Soc.* **144**(30), 13787–13793 (2022).
- ²²E. Palacios, J. A. Rodríguez-Velamazán, M. Evangelisti, G. J. McIntyre, G. Lorusso, D. Visser, L. J. De Jongh, and L. A. Boatner, “Magnetic structure and magnetocalorics of GdPO_4 ,” *Phys. Rev. B* **90**(21), 214423 (2014).
- ²³T. G. Tziotzi, D. Gracia, S. J. Dalgarno, J. Schnack, M. Evangelisti, E. K. Brechin, and C. J. Milios, “A $\{\text{Gd}_{12}\text{Na}_6\}$ molecular quadruple-wheel with a record magnetocaloric effect at low magnetic fields and temperatures,” *J. Am. Chem. Soc.* **145**(14), 7743–7747 (2023).
- ²⁴Y. Lin, J. Wang, W. Dai, K. M. Qiao, H. B. Zhou, T. Y. Zhao, F. X. Hu, and B. G. Shen, “A full solid-state conceptual magnetocaloric refrigerator based on hybrid regeneration,” *Innovation* **5**(4), 100645 (2024).

- ²⁵Z. Mo, Q. Liu, W. Hao, L. Li, H. Xie, Q. Fu, X. Gao, and J. Shen, "Magnetic properties and large low-field cryogenic magnetocaloric effect in the divalent europium borate $\text{Eu}_2\text{B}_2\text{O}_5$ compound," *Mater. Today Phys.* **41**, 101351 (2024).
- ²⁶Y. Wang, Q. Liu, L. Tian, Z. Hao, L. Zhang, Q. Fu, J. Zhao, and Z. Mo, "A cryogenic magnetic refrigerant: Magnetocaloric study of EuB_2O_4 compound," *J. Alloys Compd.* **995**, 174753 (2024).
- ²⁷C. S. Tan, "Lead-free europium and ytterbium perovskites," *RSC Adv.* **13**, 19013–19019 (2023).
- ²⁸G. T. Kent, J. Zhuang, K. R. Albanese, A. Zohar, E. Morgan, A. Kallistova, L. Kautzsch, A. A. Mikhailovsky, P. Vishnoi, R. Seshadri, and A. K. Cheetham, "Hybrid iodide perovskites of divalent alkaline earth and lanthanide elements," *J. Am. Chem. Soc.* **145**(50), 27850–27856 (2023).
- ²⁹X. Zhang, Y. Wang, X. Wu, F. Wang, Q. Ou, and S. Zhang, "A comprehensive review on mechanisms and applications of rare-earth based perovskite nanocrystals," *Chin. J. Chem.* **42**, 1032–1056 (2024).
- ³⁰J. Luo, L. Yang, Z. Tan, W. Xie, Q. Sun, J. Li, P. Du, Q. Xiao, L. Wang, X. Zhao, G. Niu, L. Gao, S. Jin, and J. Tang, "Efficient blue light emitting diodes based on europium halide perovskites," *Adv. Mater.* **33**(38), 2101903 (2021).
- ³¹A. G. Bispo-Jr, A. J. De Moraes, C. M. S. Calado, I. O. Mazali, and F. A. Sigoli, "Lanthanide-doped luminescent perovskites: A review of synthesis, properties, and applications," *J. Lumin.* **252**, 119406 (2022).
- ³²D. B. Straus, T. Klimczuk, X. Xu, and R. J. Cava, "Antiferromagnetic order in the rare-earth halide perovskites CsEuBr_3 and CsEuCl_3 ," *Chem. Mater.* **34**(23), 10772–10777 (2022).
- ³³D. G. Nocera, L. R. Morss, and J. A. Fahey, "Preparation, crystal structure, and enthalpy of formation of cesium europium(II) chloride, CsEuCl_3 ," *J. Inorg. Nucl. Chem.* **42**(1), 55–59 (1980).
- ³⁴H. Ehrenberg, H. Fuess, S. Hesse, J. Zimmermann, H. Von Seggern, and M. Knapp, "Structures of CsEuBr_3 and its degradation product $\text{Cs}_2\text{EuBr}_5 \cdot 10\text{H}_2\text{O}$," *Acta Crystallogr. B* **63**(2), 201–204 (2007).
- ³⁵C. Baopeng, W. Shihua, and Z. Xinhua, "Synthesis and structure of AEuI_3 (A—Rb, Cs) and AEuI_5 (A—K, Rb, Cs)," *J. Alloys Compd.* **181**(1–2), 511–514 (1992).
- ³⁶S.-J. Liu, T.-F. Zheng, J. Bao, P.-P. Dong, J.-S. Liao, J.-L. Chen, H.-R. Wen, J. Xu, and X.-H. Bu, "Two Gd^{III} complexes derived from dicarboxylate ligands as cryogenic magnetorefrigerants," *New J. Chem.* **39**(9), 6970–6975 (2015).
- ³⁷Y. Wang, L. Qin, G.-J. Zhou, X. Ye, J. He, and Y.-Z. Zheng, "High-performance low-temperature magnetic refrigerants made of gadolinium-hydroxy-chloride," *J. Mater. Chem. C* **4**(27), 6473–6477 (2016).
- ³⁸E. E. Oyeka, M. J. Winiarski, H. Świątek, W. Balliew, C. D. McMillen, M. Liang, M. Sorolla, and T. T. Tran, " $\text{Ln}_2(\text{SeO}_3)_2(\text{SO}_4)(\text{H}_2\text{O})_2$ (Ln=Sm, Dy, Yb): A mixed-ligand pathway to new lanthanide(III) multifunctional materials featuring nonlinear optical and magnetic anisotropy properties," *Angew. Chem. Int. Ed.* **61**(48), e202213499 (2022).
- ³⁹E. C. Koskelo, C. Liu, P. Mukherjee, N. D. Kelly, and S. E. Dutton, "Free-spin dominated magnetocaloric effect in dense Gd^{3+} double perovskites," *Chem. Mater.* **34**(7), 3440–3450 (2022).
- ⁴⁰Y. Zhang, W. Hao, J. Lin, H.-F. Li, and L. Li, "Geometrically frustrated $\text{Gd}_2\text{Ti}_2\text{O}_7$ oxide: A comprehensive exploration of structural, magnetic, and magnetocaloric properties for cryogenic magnetic cooling applications," *Acta Mater.* **272**, 119946 (2024).
- ⁴¹B. Wu, Y. Zhang, D. Guo, J. Wang, and Z. Ren, "Structure, magnetic properties and cryogenic magneto-caloric effect (MCE) in $\text{RE}_2\text{FeAlO}_6$ (RE = Gd, Dy, Ho) oxides," *Ceram. Int.* **47**, 6290–6297 (2021).
- ⁴²P. Xu, Z. Ma, P. Wang, H. Wang, and L. Li, "Excellent cryogenic magnetocaloric performances in ferromagnetic $\text{Sr}_2\text{GdNbO}_6$ double perovskite compound," *Mater. Today Phys.* **20**, 100470 (2021).
- ⁴³Y. Zhang, Y. Tian, Z. Zhang, Y. Jia, B. Zhang, M. Jiang, J. Wang, and Z. Ren, "Magnetic properties and giant cryogenic magnetocaloric effect in B-site ordered antiferromagnetic $\text{Gd}_2\text{MgTiO}_6$ double perovskite oxide," *Acta Mater.* **226**, 117669 (2022).
- ⁴⁴Z. Zhang, P. Xu, Y. Jia, and L. Li, "Structural, magnetic and magnetocaloric properties in distorted $\text{RE}_2\text{NiTiO}_6$ double perovskite compounds," *J. Phys. Energy* **5**, 014017 (2023).
- ⁴⁵Z.-J. Mo, J. Shen, L. Li, Y. Liu, C.-C. Tang, F.-X. Hu, J.-R. Sun, and B.-G. Shen, "Observation of giant magnetocaloric effect in EuTiO_3 ," *Mater. Lett.* **158**, 282–284 (2015).
- ⁴⁶B. Xu, H. Xie, Z. Mo, X. Gao, J. Wang, Z. Li, and J. Shen, "Magnetic properties and cryogenic magnetocaloric effect of pyrochlore structure $\text{RE}_2\text{Ti}_2\text{O}_7$ (RE = Gd, Tb, and Ho) compounds," *J. Appl. Phys.* **135**(7), 075104 (2024).
- ⁴⁷P. Mukherjee, Y. Wu, G. I. Lampronti, and S. E. Dutton, "Magnetic properties of monoclinic lanthanide orthoborates, LnBO_3 , Ln=Gd, Tb, Dy, Ho, Er, Yb," *Mater. Res. Bull.* **98**, 173–179 (2024).